ADVANCED FUNCTIONAL MATERIALS
www.afm-journal.de

Film-Based Implants for Supporting Neuron–Electrode Integrated Interfaces for The Brain

*Min D. Tang-Schomer, Xiao Hu, Marie Hronik-Tupaj, Lee W. Tien, Michael J. Whalen, Fiorenzo G. Omenetto, and David L. Kaplan**

Neural engineering provides promise for cell therapy by integrating the host brain with brain–machine-interface technologies in order to externally modulate functions. Long-term interfaces with the host brain remain a critical challenge due to insufficient graft cell survivability and loss of brain electrode sensitivity over time. Here, integrated neuron–electrode interfaces are developed on thin flexible and transparent silk films as brain implants. Mechanical properties and surface topography of silk films are optimized to promote cell survival and alignment of primary rat cortical cells. Compartmentalized neural cultures and co-patterned electrode arrays are incorporated on the silk films with built-in wire connections. Electrical stimulation via electrodes embedded in the films activated surrounding neurons to produce evoked calcium responses. In mice brains, silk film implants show conformal contact capable of modulating host brain cells with minimal inflammatory response and stable indwelling for weeks. The approach of combining cell therapy and brain electrodes could provide sustained functional interfaces with ex vivo control with spatial precision.

1. Introduction

Neural engineering provides promise for bringing new cures for brain disorders, and exciting approaches for brain-machine-interface technology. Brain cell therapy could allow the functional replacement of missing or damaged neurons by transplanting cells that integrate with the host brain.[1,2] For example, grafts of fetal brain tissues in epileptic patients provide inhibitory neurons to suppress abnormal seizures.[3] Alternatively, in the field of brain–machine-interfaces, brain electrodes could transmit neuronal signals as artificial circuitry to bypass a lost neuronal connection, such as the corticospinal pathway in a paralyzed patient.[4] These exciting fronts could provide opportunities for modulating brain functions at the single neuron as well as at more complex network levels. In both fields, long-term interfaces with the host brain remains a critical challenge, depending on graft cell survival for cell therapy[5,6] and sustained signal integrity for brain electrodes.[7,8] A combined approach for neuron–electrode integrated implants is an approach that could provide ex vivo control of cell grafts (i.e., survival and function), a stable graft cell–electrode interface, and support graft–host integration via intrinsic programs of synaptic formation, thereby ensuring sustained functional interfaces.

These neural engineering approaches would require new materials for supporting long-term indwelling and function of cell grafts and electrodes. The biomaterials used in such systems must be non-inflammatory to avoid an innate foreign body response such as gliosis which would result in scar formation.[9,10] This biological response would result in the rejection of grafted cell functions and loss of electrode sensitivity. In addition, it is critical for the biomaterial to have direct contact with host brain cells in order to support optimal functional interfaces. These needs can be addressed by improved material properties, including brain-compatible mechanical stiffness,[11] conformability with convoluted tissue surfaces as flexible films[12] or injectable gels,[13] and biocompatibility for neuronal growth.[14,15] For functional integration with host brain neurons it is desirable to induce guided neuronal/glial alignment and axon tract formation, such as by imparting structural anisotropy in the implant material.[16] Many biomaterials are being developed to support cell grafts in the brain,[17] or to facilitate chronic electrode implants as coatings.[18] However, a brain-implantable material to support both neurons and electrodes as sustained neuron–electrode interfaces has not been realized.

M. D. Tang-Schomer, M. Hronik-Tupaj, L. W. Tien, F. G. Omenetto, Prof. D. L. Kaplan
Tufts University
Department of Biomedical Engineering
Medford, MA, 02155, USA
E-mail: david.kaplan@tufts.edu
X. Hu
Department of Physics and Astronomy
Rowan University
Glassboro, NJ, 08028, USA
M. J. Whalen
Harvard Medical School
Acute Brain Injury Research Laboratory
Massachusetts General Hospital for Children
Charlestown, MA, 02129, USA
F.G. Omenetto
Tufts University
Physics Department
Medford, MA, 02155, USA

DOI: 10.1002/adfm.201303196

In this study, we developed a film-based biomaterial that supported integrated interfaces between fetal neuronal cells and patterned electrode arrays as brain surface implants. Silk is a biopolymer purified from silkworm cocoons and solubilized into an aqueous salt-free solution.[19] Silk materials can be processed to produce tissue-tailored mechanical properties,[20] for example, by controlling the degree of β-sheet crystallization.[21] Silk films are an appealing biomaterial for brain implant applications because they are compatible with electrode micropatterning technologies,[22,23] bioabsorbable and degradable[24,25] as indwelling chronic implants,[26] and form conformal contact with brain surfaces.[12]

Here, we sought to optimize silk film properties that could modulate primary rat cortical cell behavior, including cell survival and alignment. We further designed a controlled neuron–electrode interface by incorporating microfluidic neuronal cultures with film-based electrode patterning. Co-patterning cells and electrodes allow multiple options for targeted modulation of neuron–electrode interfaces with one implant. This work provides a prototype for developing a functional neuron–electrode integrated interface for the brain.

2. Results

2.1. Controlling Mechanical Stiffness of Silk Films to Support Neural Cell Growth

To generate films with different mechanical stiffness, we used two independent parameters during silk film processing, annealing temperature and thickness (**Figure 1**). Dried silk films produced from 1% silk fibroin solutions of 25 µL, 50 µL, and 75 µL per well of a 96-well plate were processed at 4 °C (LowT), 24 °C (RT), or 95 °C (HighT) (LowT_25, LowT_50, LowT_75, RT_25, RT_50, RT_75, HighT_25, HighT_50, HighT_75). Scanning electron microscopy (SEM) measured thicknesses were 2.40 ± 0.09, 3.27 ± 0.16, and 8.13 ± 0.13µm from 25 µL, 50 µL, and 75 µL solutions, respectively (n = 3/group) (Figure 1A, inset). AFM nano-indentation measurements of elastic (E) Young's modulus of dry silk films showed an increase from ~10 to 70 MPa as the annealing temperature was increased from 4 °C to 95 °C (Figure 1A). Lower temperature-treated films were softer as the film became thicker. For example, LowT_75 had

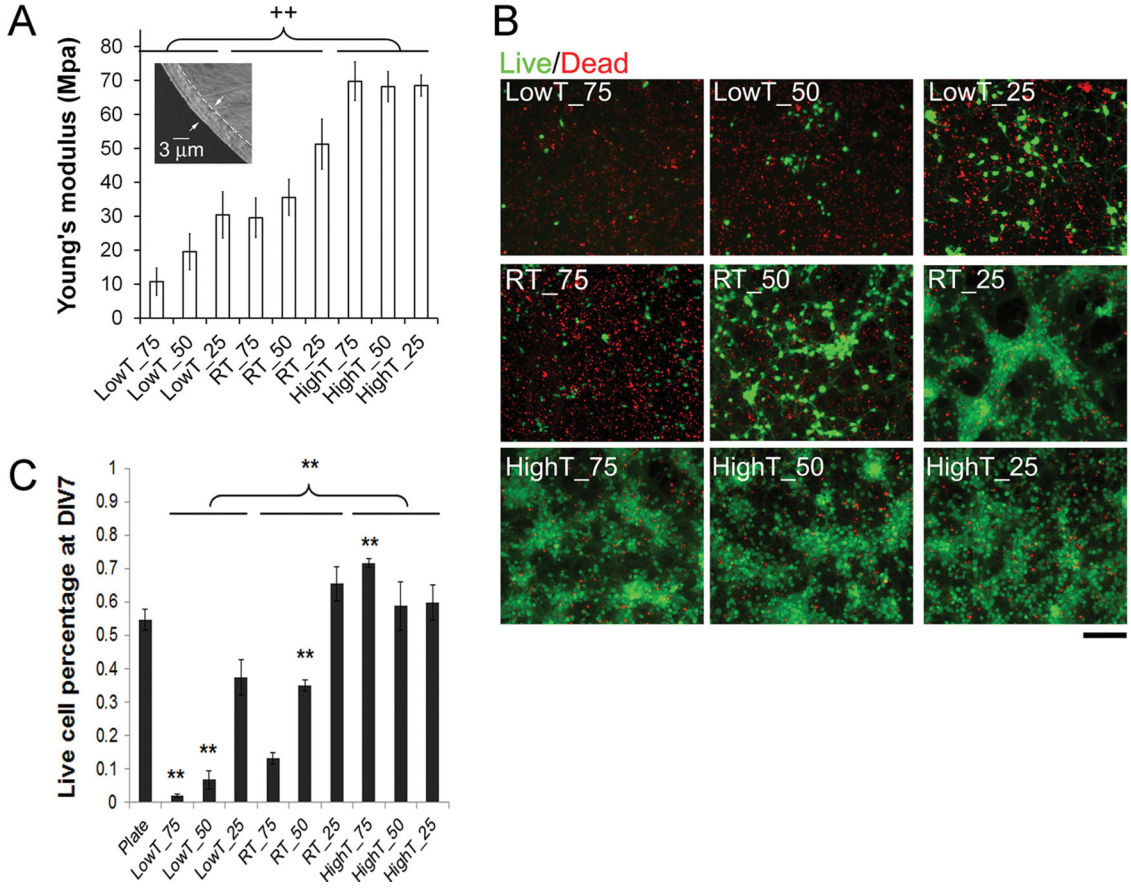

Figure 1. Primary rat cortical neural cells cultured on silk films of different elasticity. Silk film stiffness was controlled by film thickness (1% silk fibroin solutions of 25 µL, 50 µL, and 75 µL per well of a 96-well plate), and annealing temperature (4 °C, LowT; 24 °C, RT; 95 °C, HighT). A) AFM nano-indentation measured elastic (E) Young's modulus of silk films. Inset: Scanning electron microscopic (SEM) image of a fractured film showing its cross-section (arrows). Both temperature and film thickness are significant contributing factors to film elastic modulus (n = 3/group; ++, 2-way ANOVA, alpha 0.05, $p < 0.01$; Error bar, standard error of mean, s.e.m.). B) Cell viability assay of 7 day-old cultures (live cells, green; dead cells, red). Scale bar, 100 µm. C) Live cell percentages of cultures at 7 days in vitro (DIV7) (n = 3; **, $p < 0.01$ compared to Plate culture). Both temperature and film thickness are significant contributing factors to cell viability (++, 2-way ANOVA, alpha 0.05, $p < 0.01$).

a modulus of ≈10 MPa compared to LowT_25's modulus of ≈30 MPa. High temperature-treated films had a Young's elastic modulus ≈68 MPa, with no statistical difference among different thicknesses. Two-way ANOVA analysis showed that 1) within each thickness group, there were significant differences among temperature treatment, and 2) within lower temperature groups (LowT, and RT) but not the HighT group, thickness played a significant role in film elasticity ($\alpha = 0.05$; thickness, $p < 0.01$, temperature, $p < 0.01$, interaction, $p < 0.01$, $n = 3$/group). In addition, all films were found to be water-stable, as no significant weight loss was found after soaking in the PBS solution for three days.

We next determined silk film elasticity for optimal neural cell viability in vitro by comparing cultures on silk films to those in control polystyrene plates. Primary cortical cells isolated from embryonic day 18 (E18) rat brains were cultured up to 7 days. At 24 h post-seeding, all the substrates showed similar total cell numbers as well as live cell numbers (data not shown), indicating that the materials were sufficiently coated with poly-L-lycine. At day 7 in vitro (DIV7), cell viability showed an increasing trend from ≈2% to 60% as films became stiffer ($n = 3$/group) (Figure 1B,C). Low temperature-treated thicker films (LowT_75 and LowT_50) had few surviving cells (≈5%), whereas thinner ones (LowT_25) had ≈30% viability compared to the control plate (54 ± 3%, $p < 0.05$). Similarly, room temperature-treated thicker films (RT_75 and RT_50) supported significantly lower cell viabilities (13% and 35%, respectively) than the control plates ($p < 0.01$), whereas RT thinner films (RT_25) supported a cell viability of 65% ($p < 0.05$ versus control plates). High temperature-treated films had cell viabilities consistently higher of 60%, 59%, and 72% for HighT_25, HighT_50, and HighT_75, respectively, compared to 54% of the control plates ($p < 0.05$). Two-way ANOVA analysis showed a similar dependence on temperature and thickness of cell viability as film elasticity: 1) within each thickness group, there were significant differences in cell viability among different temperature treatments, and 2) within lower temperature-treated groups (LowT, and RT) but not the HighT group, thickness played a significant role in cell viability ($\alpha = 0.05$; thickness, $p < 0.01$, temperature, $p < 0.01$, interaction, $p< 0.01$, $n = 3$/group). Spearman correlation test showed a strong positive correlation of neural cell viability with film elasticity (Spearman coefficient = 0.9, $p < 0.05$).

2.2. Controlling Surface Topology of Silk Films to Direct Glial Cell Alignment

To determine how the surface topology of silk films affected neural cell alignment, primary E18 rat cortical cells were cultured on flat and patterned films with surface micro-grooves of 3 μm in width and 0.5 μm depth (**Figure 2**). The width was selected because it is comparable with the cortical axons (0.3–1 μm),[27] and glial cell processes (2–3 μm). The cultures were maintained in neuronal enriched conditions,[28] with ≈10% glial fibrillary acidic protein (GFAP)+ astrocytes and the majority (>90%) neurons. By DIV 3–5 neuronal processes stained with DiI dye were aligned with the surface microgrooves (Figure 2A). Over time as the cultures developed extensive neuronal connections, no obvious cell alignment was observed. Using immunostaining for cell type-specific markers, different behaviors of neurons and glial cells were found on silk films of a same micropattern (Figure 2B,a). Astrocyte (glial fibrillary acidic protein, GFAP+) processes were aligned with the surface microgrooves (Figure 2B,b). In contrast, neuronal (neurofilament, NF+) processes showed no particular alignment (Figure 2B,c). Furthermore, neither axons stained with β III tubulin (Figure 2B,d) nor dendrites stained with microtubule associated protein 2 (MAP2) (Figure 2B,e) showed directional preferences. In mature dense cultures, there was a considerable overlaying of GFAP+ glial cell processes with NF+ neuronal processes (Figure 2B,f), indicating that it is unlikely that the difference in alignment was due to competition for the limited numbers of surface microgrooves.

To better determine how surface topography provides directional cues for glial cell alignment, the degree of aligned processes in cortical cell cultures of different plating densities at 200–500 000 cells cm^{-2} were examined (Figure 2C,D). The densities were chosen to allow sufficient numbers of glial cells in the neuronal enriched culture. An automated ImageJ program (see Experimental Section)[29] allowed measurements of a large number of cell processes and determined the mean angles of 200k, 300k, 400k, 500k cells cm^{-2} cultures are: 91.1 ± 1.8° (n = 866, flat) versus 108.2 ± 1.1° (n = 937, microgroove angle 118°), 88.1 ± 1.7° (n = 926, flat) versus 126.3 ± 1.4° (n = 1026, microgroove angle 148°), 89.8 ± 1.7° (flat, n = 962) versus 113.9 ± 1.0° (n = 1047, microgroove angle 124°), 90.3 ± 1.5° (flat, n = 1294) versus 60.6 ± 1.8° (n = 937, microgroove angle 22°). The histogram of cultures on patterned silk films showed distinctive peaks of alignment angles (Figure 2D, right): There were ≈30% of glial processes aligned within ±9° of the surface microgrooves in all four density groups. In contrast, the angles of GFAP+ processes in flat film cultures were evenly distributed (Figure 2D, left). These data demonstrate that surface topology provides cues to direct glial cell alignment in vitro.

2.3. Microfluidic Patterned Neural Cultures on Silk Films

To generate patterned neural cultures, we adapted a compartmentalized microfluidic culture system on silk films[27]. **Figure 3**A shows the schematic of a flexible film-based implant where arrays of discrete neural cell populations are connected by a ladder of millimeter-long axon tracts. Each cell population resides on top of patterned surface electrodes (gold) on silk films. This design of neuron–electrode interfaces is distinctively different than electrode-only patterns on films (Figure 3B), as neurons (calcein AM-stained green) showed random distributions near the electrodes (dark). Figure 3C shows cell compartments co-stained with β3TB green, GFAP, red, and nuclei stain of DAPI, blue. Figure 3D shows the axon compartments of 100 μm wide and 2 mm long microchannels (calcein AM-stained green). These data demonstrate compartmentalized neural cultures on the silk films.

2.4. Film-Based Integrated Neuron–Electrode Interfaces

Figure 4 shows examples of integrated neuron–electrode interfaces on flexible and ultra-thin (2–5 μm) silk films. Electrode

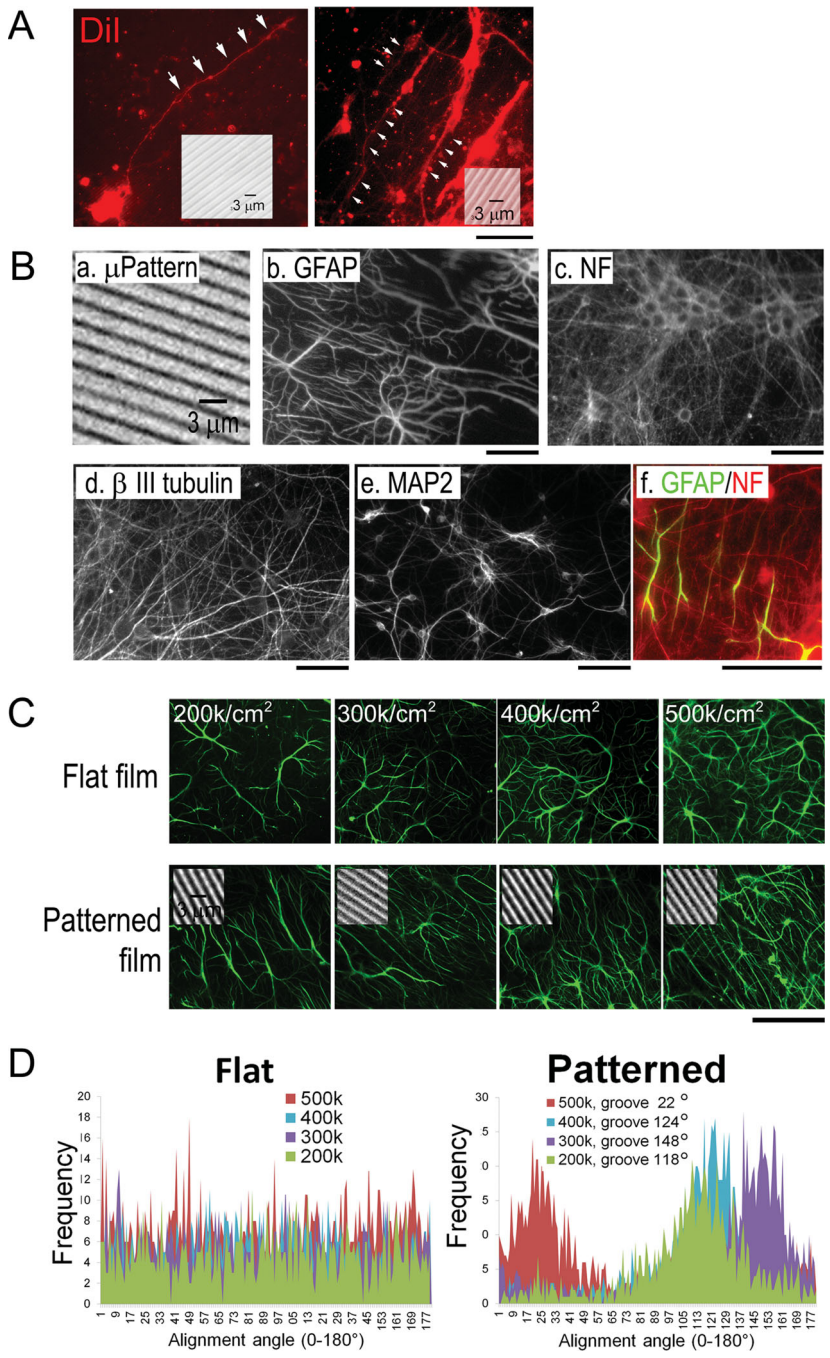

Figure 2. Primary rat cortical neural cells cultured on patterned silk films. A) Fluorescence photographs of DIV3–5 cortical cell cultures stained with DiI (red) showing axons along micro-grooves (inset) on patterned silk films. Scale bar, 100 μm. B) Fluorescence photographs of DIV16 cortical cultures on micro-grooves (a, phase contrast photograph) stained with GFAP (b), neurofilament (NF) (c), β III tubulin (d), and MAP 2 (e), respectively. Co-staining of GFAP (green) and NF (red) showed overlay of aligned glial cell processes with randomly projected neuronal processes. Scale bar, 50 μm. C) Fluorescence photographs of GFAP-immunostained DIV16 cortical cell cultures of different plating densities (indicated by the numbers) on silk films. On flat films (top), GFAP+ processes (green) showed no particular directional preferences. On patterned films (bottom), GFAP+ processes (green) showed alignment with the surface microgrooves (inset). Scale bar, 100 μm. D) Histogram of alignment angles of GFAP+ processes in cortical cell cultures of different plating densities on silk films ($n = 10$/group). On flat films (Left), there are no major peaks. On patterned films (Right), distinctive major peaks correspond to the angle of the surface groove (the groove angles were indicated in the legend).

patterning was produced by gold sputter-coating on dried silk films as previously described (Figure 4A,a). The water-annealed and detached silk films remained self-supporting, flexible, and transparent with excellent electrode patterning (Figure 4A,b). Figure 4Ac,d shows representative fluorescence images of a mature (DIV 21) calcein AM-stained (green) neuronal culture on electrode-patterned silk films, demonstrating extensive neuronal connections near the gold electrode. To build wire connections in order to interface with external electronics (Figure 4B), thin gold wires (100 μm dia.) were immersed in the silk fibroin solution in an arrangement that matched the designed gold electrode arrays prior to film drying. Figure 4 e and f show two final devices that were suspended on the surface of water droplets. Figure 4C shows models of the electric potentials (colors) and electric fields (red arrows) across the electrode-patterned silk films, as an electrical potential of 120 mV was applied at all four pairs of electrodes (g), or at an individual pair (k–l). The electric field strength in the x direction between the anode and cathode as modeled in COMSOL was 56 mV mm^{-1}, whereas that between a neighboring inactivated electrode was significantly smaller at 15 mV mm^{-1}. Oscilloscopic tests on a hydrated film in cell culture media (simulating neuron stimulation experiment) of un-stimulated pairs of electrodes obtained negligible signals compared to ≈100% signal retention between the stimulated pair of electrodes. These results demonstrate silk-film based integrated neuron–electrode interfaces with localized transmission of electric signals.

2.5. Neural Calcium Responses by Silk Film-Supported Electrical Stimulation

To demonstrate the interface functions, we examined neuronal calcium responses under electrical stimulation via silk-film embedded electrodes (**Figure 5**). Figure 5Aa shows electric modeling of a simplified version of an interface. Figure 5Ab shows a fluorescence image of neurons stained with Fluo-4 (green), a calcium indicator, overlaid with a phase-contrast image of the gold electrode (black) on the same silk film. Randomly selected neurons (individually numbered) were analyzed for their calcium levels. In a representative trial (Figure 5B), a series of biphasic square-waves of varying frequencies (20, 200, and 2000 or 2k Hz) were applied for 6 minutes

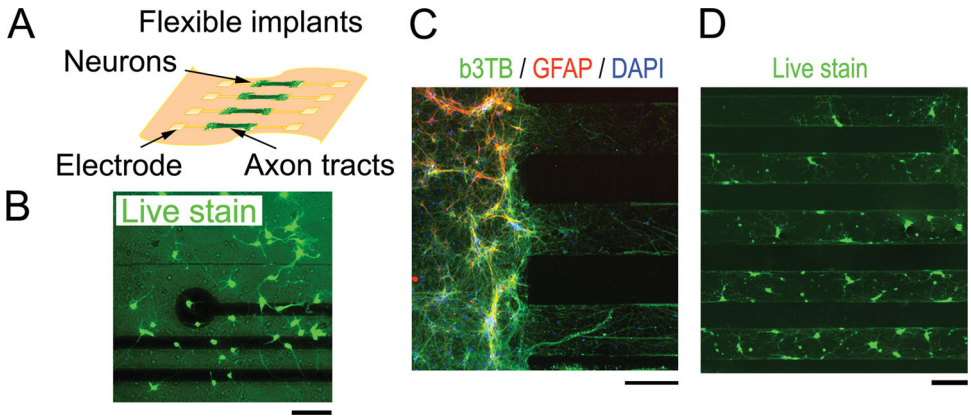

Figure 3. Microfluidic patterned neural cultures on silk films. A) Schematics of a flexible film-based implant. B) Cortical neurons growing on electrode-only patterns. Neurons (calcein AM-stained in green) showed random distribution near the electrodes (dark). Scale bar, 100 µm. C) The cell compartments (c, co-staining of β3TB green, GFAP, red, and neuclei stain of DAPI, blue), Scale bar, 100 µm. D) The axon compartments (calcein AM-stained in green, 100 µm W, 2 mm total length). Scale bar, 100 µm.

per condition, and time-lapse (per minute) fluorescence images were taken: c–f, original images; g–j, "red-hot" heatmap generated by ImageJ. Quantification of calcium signals at each time-point normalized by the base-level ("Calcium level changes") of individual neurons (as marked in b) shows three distinctive groups of neuronal responses (Figure 5C). Group analysis (Figure 5D) shows that 1) Group I neurons (8, 10, 13, 14) had significantly increased calcium levels at 20 and 200 Hz, and no changes at 2k Hz; 2) Group II neurons (1–7, 11, 12, 15) had significantly decreased calcium levels at all three frequencies; and 3) Group III neurons (9) had significantly increased calcium levels at all three frequencies. This complex heterogeneity of evoked calcium responses had been shown to depend on stimulation frequencies, duration, and neuron cultures, in repeated experiments ($n = 6$). We observed that closely clustered neurons appeared to exhibit similar responses. Notably, there was a great temporal correlation between neuronal responses and electrical stimulation. These results demonstrate a functional interface of neuron–electrode on silk films.

2.6. Silk Films as Indwelling Brain Surface Implants

To determine the feasibility of silk films for brain implants, the films were placed onto mouse brains exposed by craniotomy and glial cell responses were examined (**Figure 6**). Based on previously characterized film mechanical stiffness, we determined that films prepared with as in the RT_25 group were best suited for brain surface placement; softer and thinner films instantaneously hydrated and tore, and stiffer and thicker films were less conformal. The films immediately hydrated upon contact and "wrapped" around the brain's surface. The thin films (≈2 µm) posed no hindrance for replacement of the craniotomy skull cap (Figure 6A and B). Animals with silk film implants showed no discernible abnormal behavior compared with sham animals with craniotomy but without implants ($n > 30$). At one week after implantation, no sign of residue films was found on the brain or the inside of the skull (Figure 6B and inset).

Previous studies have reported the use of readily dissolvable silk film to support electrode–neuron interface in the brain.[12] In this study, we attempted to examine long-term indwelling of un-dissolvable silk film as a substrate to support chronic implants. For this study, we used films without electrodes. To determine whether silk films impacted the behavior of brain cells in direct contact, we examined the effect of patterned films on glial cell alignment in the brain in comparison to those with flat film implants and sham controls without film implants (Figure 6C,D). After surgical removal of the dura mater, micro-patterned silk films were placed in direct contact with the cortex. GFAP immunostaining was used to determine the response of reactive glial cells up to 14 days after surgery[30] (Figure 6C,D, green). In intact brains with silk film implants, GFAP staining showed a uniform pattern throughout the cortex (Figure 6B,a) with no obvious hyper-intensity associated with gliosis near the implant site (arrows). In duratomized (DuraX) brains without film implants (Figure 6C, b), GFAP+ processes were organized randomly. The normal looking GFAP+ staining under a smooth cortical surface in non-duratomized brains with flat film implants indicated little foreign-body-reaction towards the silk material from intact dura and neural cells (Figure 6C,c); non-duratomized brains with patterned films showed similar findings (data not shown). In contrast, increased GFAP intensity and disorganization related to duratomy were observed with or without silk films (Figure 6C,d vs b,*). In duratomized brains with patterned silk films, GFAP+ processes in the superficial layers of the cortex were aligned in parallel (Figure 6C,e,f, arrows). Quantification of the angles showed that GFAP+ processes in the superficial layers were within 7 ± 1° of the cortical surface of the brains with patterned film implants versus 76 ± 6° of the brains with flat film implants ($n = 3$ per group, $p < 0.01$). These data suggest that silk film implants can form direct contacts with the host brain at the cell level and potentially modulate the graft–brain interface.

3. Discussion

In the field of cell grafts and implantable electrodes for the brain, long-term interfaces with the host brain remain a critical

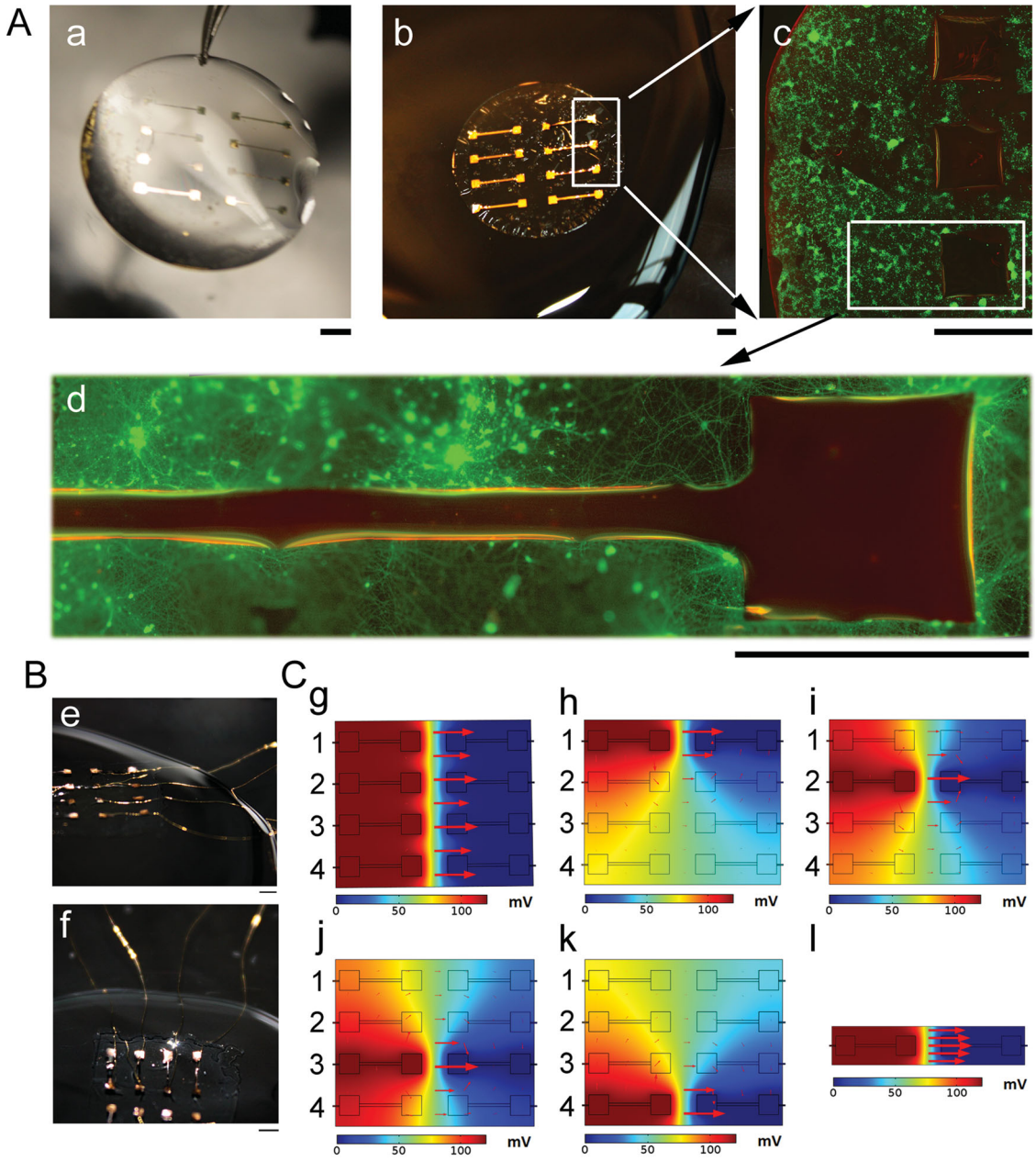

Figure 4. Film-based integrated neuron–electrode interfaces. A) Examples of integrated neuron–electrode interfaces on flexible and ultra-thin (2–5 μm) silk films (15 mm dia.) a) Electrode patterning on dried silk films supported by a glass coverslip. b) Detached silk films with electrode patterning. c,d) Representative fluorescence images of a mature (DIV 21) calcein AM-stained (green) neural cell culture on electrode-patterned silk film. Scale bar, 2 mm. B) Patterned silk films with built-in gold wire connections (100 μm dia.) suspended on water droplets. Scale bar, 2 mm. C) Electric modeling of electrode-patterned silk films. An electric potential of 120 mV was simulated at all four pairs of electrodes (g), or at an individual pair ("pair 1", h; "pair 2", i; "pair 3", j; "pair 4", k; any one pair, l). Electric potentials in mV are shown in colors. Electric field strength and directions are illustrated by the red arrows. Arrow size is proportional to electric field strength.

challenge. Here, silk film-based implants were developed to support integrated neuron–electrode interfaces. Mechanical properties and surface topography of silk films were optimized to promote cell survival and alignment of primary rat cortical cells. Further control of co-patterned neuronal connections and electrodes could allow multiple options for targeted modulation of neuron–electrode interfaces within a single implant. In live mice, silk film implants on brains showed conformal contacts capable of modulating host brain cells with minimal inflammatory response and stable indwelling for weeks. These results demonstrate a prototype for developing functional neuron–electrode integrated brain–machine-interfaces. The approach of combining cell therapy and brain electrodes could potentially provide sustained functional brain-machine

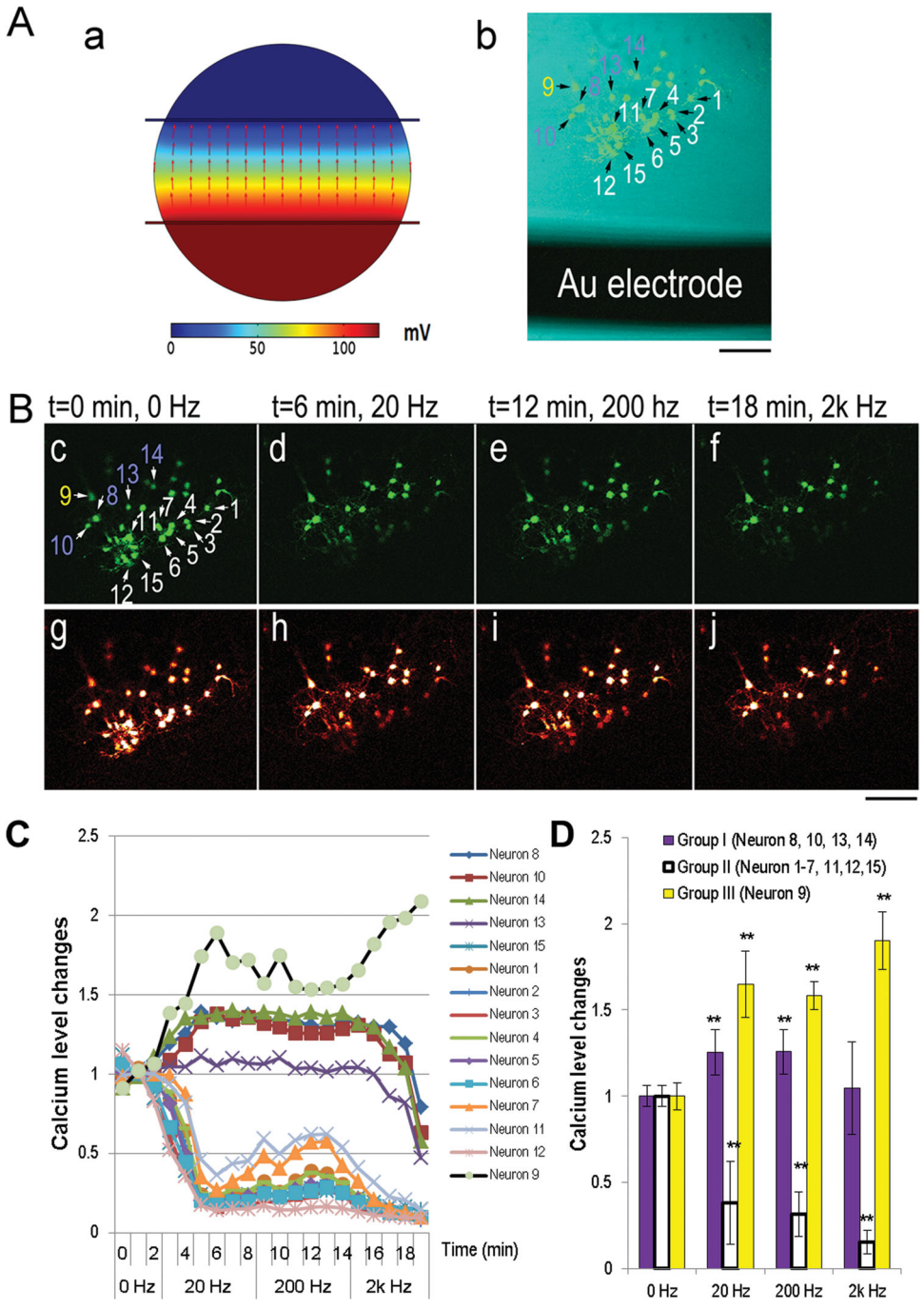

Figure 5. Neural calcium responses by silk film-supported electrical stimulation. A) A simplified version of a silk film-supported neuron–electrode interface. a) Electric modeling a pair of gold electrode (6 mm apart) embedded in a 15 mm dia. silk film. b) Fluorescence image of neurons stained with Fluo-4 (green), a calcium indicator, overlaid with a phase-contrast image of the gold electrode (black) on a same silk film. Scale bar, 100 µm. B) Time-lapse fluorescence images of neurons under stimulation of a series of biphasic square-waves of varying frequencies of 20, 200, and 2000 (2k) Hz. c–f) original images; g–j) "red-hot" heatmap generated by NIH ImageJ program. Scale bar, 100 µm. C) Quantification of calcium signals at each time-point normalized by the base-level ("Calcium level changes") of individual neurons (as marked in b). D) Quantitative analysis of averaged group responses: Group I, neuron 8, 10, 13, 14; Group II neuron 1–7, 11, 12, 15; Group III neuron 9. Student's t-test, **, $p < 0.01$ compared to 0 Hz (the baseline).

interfaces with ex vivo control of neuron–electrode interface with spatial precision.

Silk films of micro-scale thickness are mechanically robust, strong enough to be self-supporting, and flexible enough to conform to complex tissue surfaces.[31] Unlike dissolvable silk films that were used to maximize contact between the surface electrodes and the brain;[31] films used in this study were intended to be water-stable in order to support longer-term

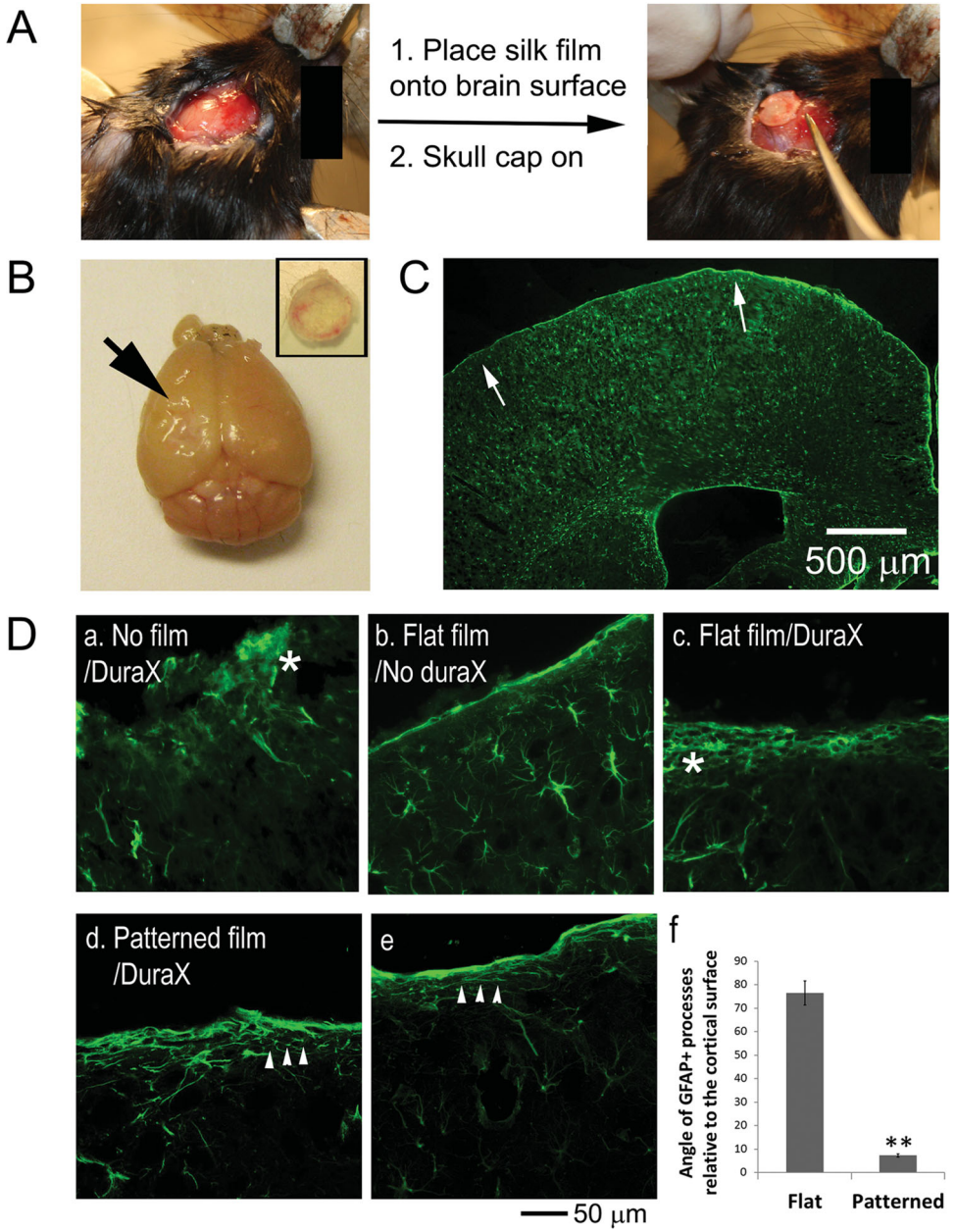

Figure 6. Patterned silk films direct alignment of reactive glial cells in the brain. A) Upon placement of a thin silk film (≈2 μm) onto the exposed brain surface after craniotomy, the film immediately hydrated upon contact and "wrapped" around the curved surface (left). The bone flap was replaced at the craniotomy site (right). B) Macroscopic view of the brain with silk film at 1 week post-implantation with no visible sign of residue silk material on the brain surface (arrow) or the inside of the skull cap (inset). C) Representative fluorescence photograph of brain coronal sections showing uniform GFAP staining (green) near the implant site (arrows) and throughout the cortex. Scale bar, 500 μm. D) Representative fluorescence photographs of GFAP-stained coronal sections of the cortex at 2 week post-implantation of duratomized (DuraX) brain without film (a), intact brain with flat film (b), duratomized brain with flat film (c), and duratomized brain with patterned film (d,e). Gliosis was manifested as increased intensity and disorganized pattern of GFAP+ staining (*). Aligned GFAP+ processes were marked with arrowheads. Scale bar, 50 μm. f) Quantification of alignment angles of GFAP+ processes relative to the cortical surface of brains with flat film vs patterned film implant ($n = 3$/group, Student's t-test, ** $p < 0.01$).

stability of the implanted neuron–electrode interface. For this purpose, silk films were treated by water annealing to render them insoluble, whereas film elasticity was controlled by modulations of film thickness and annealing temperature. This processing is based on temperature-controlled regulation of water vapor to control silk crystallization, that is, the content of β-sheet structure, which contributes to the material stiffness. According to our previous studies,[32] low temperature (4 °C) water vapor annealing physically crosslinks the silk molecules (molecular weight ≈400k Da) via beta-sheet crystals at about 15–20%, along

with significant alpha-helix. These dense structures reduce or eliminate the release of long chain proteins (including silk) from the bulk films.[33,34] The water-stability of the films used in this study was found to be similar to our previous data.[33] Thicker films yielded a softer modulus than thinner films at 4 °C and 37 °C, but not at 95 °C. Theoretically, the elastic modulus for perfect bulk materials should not be affected by the film size or thickness. The thickness dependence may be related to the bound water network,[35] typical of protein-based materials such as silk.[32]

The finding of a positive correlation of neural cell viability with silk film elasticity is consistent with the biomechanical sensitivity of neural cells.[36–38] However, the modulus of hydrated silk materials onto which the cells were in contact will need further characterization in future studies in order to compare such responses with more commonly used hydrogel-based systems.[37,38] Nevertheless, the highly tunable modulation of material elasticity shows a unique advantage of applying this system for modulating neural cell-material interface behaviors.

This study provides two methods for controlled cell alignment on silk films, as surface microgrooves for glial cells and as microfluidic substrates for axon connections. Silk films can be patterned in submicron- and micron scales in a straightforward micro-molding process in a dry state,[23] and faithfully retain the surface topography after hydration.[39] The present study showed that micro-patterned silk films are capable of inducing the alignment of astrocytes and nascent neuronal processes, but not mature axons. The finding of nascent neurite alignment was consistent with other reports of surface pattern-guided axon outgrowth.[40–42] For mature axon connections, however, the data indicate that monolithic topology presented on a 2D surface may be insufficient. By contrast, physical confinement by microfluidic channels (or tunnels) is more effective for patterning long-distance axon tracts.[27] In future studies, these properties could be incorporated in one implant to modulate multiple cells at the graft-host interface in the brain. Notably, the compatibility of silk films with micropatterning and microfluidic technologies[23] could allow a wide range of neural circuit designs.

The neuron–electrode interface function was demonstrated by evoked calcium responses of the neurons in vitro. Electrical stimulation transmitted by silk-film embedded electrodes elicited calcium level changes that correlated with stimulation conditions including timing, frequency and duration. These changes showed heterogeneous responses among individual neurons, potentially reflecting the complexity of local circuitries and dynamics of signal propagation.[43–46] Our previous study showed that chronic electrical stimulation via silk film-supported interface can promote neurite outgrowth and alignment.[47] Combining these technologies, an integrated neuron–electrode interface could potentially promote the formation of a pre-determined neural network, as a functional replacement of damaged cortical circuits in the brain. As a first step towards this goal, it is necessary to examine whether the in vitro developed interface could be implanted into the brain and maintain long-term biocompatibility.

The feasibility of silk films as indwelling brain implants for supporting cell grafts and/or electrodes was demonstrated with the in vivo studies. Silk films elicited little inflammatory response after weeks in the brain; in addition, glial cells aligned at the interface via the surface microgrooves. These data demonstrate excellent contact of the film implant with individual host brain cells, suggesting promising potential for film-based cell grafts for brain integration.

These studies provide an approach for developing integrated neuron–electrode implants for the brain. Further, the capability of independent and simultaneous modulation of different neuron/electrode pairs within one implant could allow many different design features to tailor region-specific interface applications. These properties could provide a path for ex vivo control of graft cell-electrode interfaces with spatial precision, therefore ensuring sustained functional interfaces.

4. Experimental Section

Silk Film Preparation: Cocoons of *B. mori* silkworm (Tajima Shoji Co., Yokohama, Japan) were boiled for 20 min in 0.02 M $Na_2CO_3$and rinsed to extract the glue-like sericin from the structural fibroin proteins.[19] The fibroin extract was dissolved in a 9.3 M LiBr solution at 60 °C for 4–6 h and then dialyzed in distilled water using Slide-a-Lyzer dialysis cassettes (Pierce, MWCO 3500) for 2 days. After centrifugation (13 000 g, 20 min) to remove insoluble residues, a 5–8% (wt/vol) silk fibroin solution was obtained and stored at 4 °C. Silk films were produced by casting 100 µL sterile-filtered silk fibroin solution (1–2%) onto polydimethylsiloxane (PDMS) (Sylgard 184; Dow Corning, Midland, MI, USA) molds (14 mm dia., 0.5–1 mm thick), or directly cast in polystyrene culture plates (65 µL cm^{-2}), and drying in a fume hood overnight. The films were rendered water-insoluble by β-sheet formation via water annealing in a water-filled desiccator for >5 h.[32,42,48]

Silk Films with Controlled Mechanical Stiffness: Temperature-controlled β sheet formation was used to produce silk films of different Young's modulus (10–100 Mpa).[32] Dried silk fibroin films produced from 1% (wt/vol) silk fibroin solutions were processed at 4 °C (LowT), 24 °C (RT), and 95 °C (HighT), respectively. Elastic (*E*) Young's modulus of silk films was measured via nano-indentation using atomic force microscopy (AFM), described by the Hertz model:

$$F = (2/\pi)[E/(1 - \nu^2)]\, \delta^2 \tan(\alpha)$$

Where *F* is the loading force, given by the deflection (*d*) of the cantilever multiplied by the force constant *k* (3.152 N m^{-1}) of the cantilever: $F = kd$, whereas *d* is given as the sample height (*z*) minus the indentation depth (δ). ν is the Poisson ratio assumed as 0.5 given the rubber-like elasticity of protein films. α is the half-opening angle (20°) of the cylindrical cone for the AFM tip. Nine measurements were made from three identical films per group.

Films from corresponding solutions of 25 µL, 50 µL, and 75 µL per well of a 96-well plate were prepared separately for thickness measurement. Films were fractured to expose the cross sections and examined with a field emission scanning electron microscope (Zeiss EVO10, Carl Zeiss, Germany). For each film, three measurements from randomly selected regions were made.

Silk Films with Controlled Surface Topography: To prepare films with controlled surface topography, flat and patterned PDMS molds were prepared by casting on flat optical mirror and 600 lines mm^{-1} diffraction grating (Edmund Optics, Inc. Barrington, NJ, USA) surfaces, respectively, as previously described.[23,43,49] For this study, films generated from patterned PDMS molds had microgrooves of 3 µm in width and 0.5 µm in height. Films were transferred to polystyrene plates, and prepared for cell culture of plating densities at 200, 300, 400 and 500 000 cells cm^{-2}. For in vitro studies, four identical cultures per condition (density, time point) were prepared. For in vivo studies, three animals per group (patterned vs flat films) were used.

Silk Films as Substrates for Microfluidic Systems and Patterned Multi-Electrode Arrays: Thin silicone mask was prepared to generate

microfluidic systems, as previously described. Polydimethylsiloxane (PDMS, Sylgard 184, Dow Corning, MI, USA) was spin-coated (Model WS-400B-6NPP/LITE, Laurell Technologies Corp., North Wales, PA, USA) onto silicon wafers, cured, and peeled off the wafer. A silk film made conformal contact with a PDMS film-mask, and was sputter-coated with gold (60–100 nm thickness) using a NSC-3000 sputter coater (Nano-Master Inc., Austin, TX, USA). Patterned silk films were subsequently water-annealed, UV sterilized, and coated with 20 μg mL^{-1} poly-L-lysine (Sigma-Aldrich, St. Louis, MO, USA) overnight, washed and dried prior to introducing cells. To connect gold wires into patterned silk films, thin gold wires (0.005 inch dia., Surepure Chemetals Inc., Florham Park, NJ, USA) were threaded through a PDMS film mask and immersed in silk solution, prior to film drying. The wires were embedded in dried silk films after removal from the PDMS mask.

Electric Field Modeling: Electric potential and electric field strength was modeled across stimulated silk films using the electrostatics analysis module in COMSOL Multiphysics software (version 4.3b, COMSOL Inc., Burlington, MA). COMSOL Multiphysics solved for electric potential (mV) and electric field strength (V m^{-1}) using finite element analysis methods and the following equation: $E = -\nabla V$; where E = electric field strength (V m^{-1}), V = applied max voltage (A Ω). Briefly, the gold electrode sputtered silk films were drawn to scale using COMSOL's geometry feature and the anode and cathode were designated for each simulation. The geometry was meshed extra finely as a free tetrahedral having a maximum and minimum element size as 0.539 and 0.0231 mm, respectively. The stimulus applied to all models was 0.120 V at 20, 200, and 2000 Hz frequencies.

Primary Cortical Cell Isolation and Culture: The brain tissue isolation protocol was approved by Tufts University Institutional Animal Care and Use Committee and complies with the NIH Guide for the Care and Use of Laboratory Animals (IACUC # B2011-45). Primary rat cortical neural cell culture was prepared as previously reported.[27] Briefly, cortices from embryonic day 18 (E18) Sprague Dawley rats (Charles River, Wilmington, MA, USA) were isolated, dissociated with trypsin (0.3%, Sigma) and DNase (0.2%, Roche Applied Science, Indianapolis, IN, USA) followed with trypsin inhibition with soybean proteins (1 mg mL^{-1}, Sigma), centrifuged, and plated at 200–625 000 cells cm^{-2} in NeuroBasal media (Invitrogen, Carlsbad, CA, USA) supplemented with B-27 neural supplement, penicillin/streptomycin (100 U mL^{-1} and 100 μg mL^{-1}), and GlutaMax (2 mM) (Invitrogen). Cultures were maintained in 37°C, 100% humidity and 5% CO^2in an incubator (Forma Scientific, Marietta, OH, USA) for up to 16 days in vitro (DIV 1–16). Substrates were coated with poly-L-lysine (Sigma, 20 μg mL^{-1}) overnight and washed extensively before cell plating.

Cell Viability Assay: Cell viability was assessed using the LIVE/DEAD Viability Assay Kit (Invitrogen). Briefly, culture media was replaced with Dulbecco's phosphate-buffered saline (DPBS; Invitrogen) containing calcein AM (4 μM) and ethidium homodimer-1 (2 μM). After 30 min incubation at 37 °C, the cells were changed into fresh culture media, and viewed under a fluorescence microscope (Leica DM IL; Leica Microsystems, Wetzlar, Germany) equipped with a digital camera (Leica DFC340 FX). Fluorescence images were acquired using excitation at 470 ± 20 nm and emission at 525 ± 25 nm for live cells, and excitation at 560 ± 20 nm and emission at 645 ± 40 nm for dead cells, respectively. NIH ImageJ software was used to quantify cell numbers.

Immunocytochemistry and Image Analysis: Cells were fixed with 4% paraformaldehyde (Fisher Scientific, Pittsburgh, PA, USA) for 20 min, washed, permeabilized and blocked with 0.1% Triton X-100 (Fisher Scientific) including 4% goat serum (Sigma) for 20 min, followed with incubation of primary antibodies overnight at 4 °C. After three 10 min washes, cells were incubated with secondary antibodies for 1 h at room temperature, followed by extensive washes. Antibodies included: anti-glial fibrillary acidic protein (GFAP, mouse, 1:1000; rabbit, 1:500; Sigma), anti-neurofilament 200 (NF, rabbit, 1:500; Sigma), anti-βIII-tubulin (b3TB, rabbit, 1:500; Sigma), anti-microtubule associated protein 2 (MAP2, mouse, 1:1000; Sigma). Goat anti-mouse or rabbit Alexa 488 and 568 (1:250; Invitrogen) secondary antibodies were used. Fluorescence images were acquired on a Leica DM IL fluorescence microscope with excitation at 470 ± 20 nm and emission at 525 ± 25 nm for Alexa 488, and excitation at 560 ± 20 nm and emission at 645 ± 40 nm for Alexa 568.

To quantify alignment of GFAP-positive glial processes on patterned silk films, a custom-made Image J plugin based on NeurphologyJ[29] was used. Glial processes were defined as GFAP- positive spindle-shaped profiles with ≥15 μm length and 0–0.5 circularity. For each condition, ten 100× fields (638 μm × 478 μm) from four identical cultures were collected, each field containing ≈100 processes.

Electrical Stimulation: A function generator (Tenma Universal Test Center 72–5085, MCM Electronics, Centerville OH, USA) delivered stimulus signals consisting of biphasic square waves of 120-160 mV (peak-to-peak) at 20, 200, or 2000(2k) Hz. Voltage applied across each silk film was verified prior to stimulation. No cellular damage was observed within the time-window of the stimulation experiment.

Calcium Imaging and Image Analysis: Calcium dye Fluo-4 AM (Invitrogen) was used to visualize changes in intracellular calcium concentration. Cultures were loaded with 1 μg mL^{-1} dye solution in controlled saline solution (CSS; 120 mM NaCl, 5.4 mM KCl, 0.8 mM MgCl2, 1.8 mM $CaCl^2$, 15 mM glucose, and 25 mM HEPES, pH 7.4) at 37 °C for 30 min, washed with CSS, and incubated in fresh media for another 30 min. Time-lapse fluorescence images were acquired every minute under the same optical settings (at Ex/Em of 488/525 nm) and imaging conditions using a confocal microscope (Leica TCS SP2, Leica Microsystems, Wetzlar, Germany). NIH Image J program was used to quantify fluorescence intensity as the mean of a region of interest (ROI) that was marked for each individual cell. Calcium level changes were quantified as the fluorescence intensity at each time point divided by the mean of baseline (i.e., at 0 Hz stimulation) fluorescence intensities

Silk Film Implantation onto Mice Brain Surface: The implantation and the trauma protocol were approved by the Massachusetts General Hospital Institutional Animal Care and Use Committee and comply with the NIH Guide for the Care and Use of Laboratory Animals. Mice (CL7/BL6, 3 months of age, Jackson Laboratories, Bar Harbor, ME) were anesthetized with 4% isoflurane, 70% N^2O and balance O^2 and positioned in a stereotaxic frame. Blow by anesthesia was maintained via a nose opening in the tubing leading from the anesthesia box and isoflurane was titrated to quiet respirations and lack of toe pinch response at a level that avoids hypotension.[50] A 5-mm craniotomy was made using a portable drill and trephine over the left parietotemporal cortex (the center of the coordinates of craniotomy relative to bregma: 1.5 mm posterior, 2.5 mm lateral), and the bone flap was removed (craniotomy). A 5-mm diameter silk film was placed on top of the exposed brain surface within the burr hole opening. The craniotomy was replaced and the scalp was sutured closed. Mice returned to their cages to recover from anesthesia. For implants of patterned films and control flat films, the dura mater was surgically removed by gently rubbing the exposed surface with a sterile Q-tip until the blood vessels underneath the dura became clear visually.

Assessment of Glial Cell Alignment in Brains with Patterned Silk Film Implants: At 14 days after implant surgery, mice were anesthetized with isoflurane and transcardially perfused with 4% paraformaldehyde. Fixed brains were dehydrated with 30% (wt/wt) sucrose overnight, and transferred to phosphate-buffered saline (PBS; pH 7.4) solution. Coronal brain sections (14 μm) were cut at 150 μm interval. The sections were blocked in 0.1% Triton X-100 (Fisher Scientific) with 4% goat serum (Sigma) for 20 min, and incubated with rabbit anti-glial fibrillary acidic protein (GFAP) (1:1000; Sigma) overnight at 4 °C. After three 10 min washes, sections were incubated with goat anti-rabbit Alexa 568 (1:250; Invitrogen) secondary antibodies for 1hr at room temperature. The sections were washed in PBS and cover-slipped with Fluoromount (Invitrogen). Fluorescence images were acquired on a Leica DM IL fluorescence microscope with excitation at 540 nm and emission at 680 nm. NIH ImageJ program was used to quantify alignment of GFAP-positive glial processes. Four 200× microscopic fields (638 μm × 479 μm) from three sections per animal were analyzed.

Statistical Analysis: Data are mean ± standard error of mean (S.E.M.). Analysis of silk film elastic modulus and cell viability on soft/stiff films used two-way ANOVA. Correlation analyses used Spearman's test. PI-positive cell counts were analyzed by Student's t-test. For all tests, $p < 0.05$ was considered significant

Acknowledgements

The authors thank Gregory Frost and Dr. Steve Moss's laboratory at Tufts Center of Neuroscience for providing embryonic rat brain tissues. This work was funded by NIH (P41 Tissue Engineering Resource Center EB002520, D.L.K.), 5RO1NS061255 (M.J.W.), and Tufts Center for Neuroscience Research Core Award to M.D.T. Preliminary work pertaining to compartmentalized neural cultures was carried out by M.D.T. in Dr. Douglas Smith's laboratory at the University of Pennsylvania.

Received: September 15, 2013
Revised: September 30, 2013
Published online: November 18, 2013

[1] O. Lindvall, A. Bjorklund, **2004**, *1*, 379–381.
[2] G. J. Delcroix, P. C. Schiller, J. P. Benoit, C. N. Montero-Menei, *Biomaterials* **2010**, *31*, 2105–2120.
[3] A. K. Shetty, *Neurotherapeutics* **2011**, *8*, 721–735.
[4] M. A. Nicolelis, *Nat. Rev. Neurosci.* **2003**, *4*, 417–422.
[5] A. Bjorklund, U. Stenevi, R. H. Schmidt, S. B. Dunnett, F. H. Gage, *Acta Physiol. Scand. Suppl.* **1983**, *522*, 9–18.
[6] V. Darsalia, S. J. Allison, C. Cusulin, E. Monni, D. Kuzdas, T. Kallur, O. Lindvall, Z. Kokaia, *J. Cereb. Blood Flow Metabol.* **2011**, *31*, 235–242.
[7] R. W. Griffith, D. R. Humphrey, *Neurosci. Lett.* **2006**, *406*, 81–86.
[8] B. C. Lega, M. D. Serruya, K. A. Zaghloul, *Crit. Rev. Biomed. Eng.* **2011**, *39*, 5–28.
[9] J. W. Fawcett, R. A. Asher, *Brain Res. Bull.* **1999**, *49*, 377–391.
[10] M. V. Sofroniew, *Trends Neurosci.* **2009**, *32*, 638–647.
[11] P. Moshayedi, F. Costa Lda, A. Christ, S. P. Lacour, J. Fawcett, J. Guck, K. Franze, *J. Phys. Condensed Matter.* **2010**, *22*, 194114.
[12] D. H. Kim, J. Viventi, J. J. Amsden, J. Xiao, L. Vigeland, Y. S. Kim, J. A. Blanco, B. Panilaitis, E. S. Frechette, D. Contreras, D. L. Kaplan, F. G. Omenetto, Y. Huang, K. C. Hwang, M. R. Zakin, B. Litt, J. A. Rogers, *Nat. Mater.* **2010**, *9*, 511–517.
[13] J. Zhong, A. Chan, L. Morad, H. I. Kornblum, G. Fan, S. T. Carmichael, *Neurorehabil. Neural Repair* **2010**, *24*, 636–644.
[14] M. S. Shoichet, C. C. Tate, M. D. Baumann, M. C. LaPlaca, in *Indwelling Neural Implants: Strategies for Contending with the In Vivo Environment* (Ed: W. M. Reichert), Taylor & Francis Group, LLC, Boca Raton, FL **2008**.
[15] D. Y. Wong, P. H. Krebsbach, S. J. Hollister, *J. Neurosurg.* **2008**, *109*, 715–722.
[16] D. Hoffman-Kim, J. A. Mitchel, R. V. Bellamkonda, *Annu. Rev. Biomed. Eng.* **2010**, *12*, 203–231.
[17] G. Orive, E. Anitua, J. L. Pedraz, D. F. Emerich, *Nat. Rev. Neurosci.* **2009**, *10*, 682–692.
[18] L. Tien, F. Wu, M. Tang-Schomer, E. Yoon, F. Omenetto, D. Kaplan, *Adv. Funct. Mater.* **2013**, *23*, 3185–3193.
[19] D. N. Rockwood, R. C. Preda, T. Yucel, X. Wang, M. L. Lovett, D. L. Kaplan, *Nat. Protoc.* **2011**, *6*, 1612–1631.
[20] F. Omenetto, D. Kaplan, *Sci. Am.* **2010**, *303*, 76–77.
[21] H. J. Jin, D. L. Kaplan, *Nature* **2003**, *424*, 1057–1061.
[22] D. H. Kim, Y. S. Kim, J. Amsden, B. Panilaitis, D. L. Kaplan, F. G. Omenetto, M. R. Zakin, J. A. Rogers, *Appl. Phys. Lett.* **2009**, *95*, 133701.
[23] J. J. Amsden, P. Domachuk, A. Gopinath, R. D. White, L. D. Negro, D. L. Kaplan, F. G. Omenetto, *Adv. Mater.* **2010**, *22*, 1746–1749.
[24] B. Panilaitis, G. H. Altman, J. Chen, H. J. Jin, V. Karageorgiou, D. L. Kaplan, *Biomaterials* **2003**, *24*, 3079–3085.
[25] R. L. Horan, K. Antle, A. L. Collette, Y. Wang, J. Huang, J. E. Moreau, V. Volloch, D. L. Kaplan, G. H. Altman, *Biomaterials* **2005**, *26*, 3385–3393.
[26] E. M. Pritchard, C. Szybala, D. Boison, D. L. Kaplan, *J. Controlled Release* **2010**, *144*, 159–167.
[27] M. D. Tang-Schomer, A. R. Patel, P. W. Baas, D. H. Smith, *FASEB J.* **2010**, *24*, 1401–1410.
[28] G. J. Brewer, J. R. Torricelli, E. K. Evege, P. J. Price, *J. Neurosci. Methods* **1993**, *35*, 567–576.
[29] S. Y. Ho, C. Y. Chao, H. L. Huang, T. W. Chiu, P. Charoenkwan, E. Hwang, *BMC Bioinformatics* **2011**, *12*, 230.
[30] D. J. Myer, G. G. Gurkoff, S. M. Lee, D. A. Hovda, M. V. Sofroniew, *Brain* **2006**, *129*, 2761–2772.
[31] D. H. Kim, J. Viventi, J. J. Amsden, J. Xiao, L. Vigeland, Y. S. Kim, J. A. Blanco, B. Panilaitis, E. S. Frechette, D. Contreras, D. L. Kaplan, F. G. Omenetto, Y. Huang, K. C. Hwang, M. R. Zakin, B. Litt, J. A. Rogers, *Nat. Mater.* **2010**, *9*, 511–517.
[32] X. Hu, K. Shmelev, L. Sun, E. Gil, S. Park, P. Cebe, D. Kaplan, *Biomacromolecules* **2011**, *12*, 1686–1696.
[33] Q. Lu, X. H. Zhang, X. Hu, D. L. Kaplan, *Macromol. Biosci.* **2010**, *10*, 289–298.
[34] Q. Lu, X. Hu, X. Q. Wang, J. A. Kluge, S. Z. Lu, P. Cebe, D. L. Kaplan, *Acta Biomater.* **2010**, *6*, 1380–1387.
[35] J. Wang, F. G. Shi, T. G. Nieh, B. Zhao, M. R. Brongo, S. Qu, T. Rosenmayer, *Scipt. Mater.* **1999**, *42*, 687–694.
[36] D. E. Discher, P. Janmey, Y. L. Wang, *Science* **2005**, *310*, 1139–1143.
[37] P. C. Georges, W. J. Miller, D. F. Meaney, E. S. Sawyer, P. A. Janmey, *Biophys. J.* **2006**, *90*, 3012–3018.
[38] K. Saha, A. J. Keung, E. F. Irwin, Y. Li, L. Little, D. V. Schaffer, K. E. Healy, *Biophys. J.* **2008**, *95*, 4426–4438.
[39] E. S. Gil, S. H. Park, J. Marchant, F. Omenetto, D. L. Kaplan, *Macromol. Biosci.* **2010**, *10*, 664–673.
[40] D. Kleinfeld, K. H. Kahler, P. E. Hockberger, *J. Neurosci.* **1988**, *8*, 4098–4120.
[41] D. A. Stenger, J. J. Hickman, K. E. Bateman, M. S. Ravenscroft, W. Ma, J. J. Pancrazio, K. Shaffer, A. E. Schaffner, D. H. Cribbs, C. W. Cotman, *J. Neurosci. Methods* **1998**, *82*, 167–173.
[42] D. Y. Fozdar, J. Y. Lee, C. E. Schmidt, S. Chen, *Biofabrication.* **2010**, *2*, 035005.
[43] W. Hild, *Zeitschrift für Zellforschung und Mikroskopische Anatomie* **1966**, *69*, 155–188.
[44] S. Marom, D. Eytan, *Prog. Brain Res.* **2005**, *147*, 189–199.
[45] Y. Jimbo, Y. Tateno, H. P. C. Robinson, *Biophys. J.* **1999**, *76*, 670–678.
[46] M. Chiappalone, M. Bove, A. Vato, M. Tedesco, S. Martinoia, *Brain Res.* **2006**, *1093*, 41–53.
[47] M. Hronik-Tupaj, W. Raja, M. D. Tang-Schomer, F. Omenetto, D. Kaplan, *J. Biomed. Mater. Res.: Part A* **2012**, *101A*, 2559–2572.
[48] H. Jin, J. Park, V. Karageorgiou, U. Kim, R. Valluzzi, P. Cebe, D. Kaplan, *Adv. Funct. Mater.* **2005**, *15*, 1241–1247.
[49] E. S. Gil, B. B. Mandal, S. H. Park, J. K. Marchant, F. G. Omenetto, D. L. Kaplan, *Biomaterials* **2010**, *31*, 8953–8963.
[50] D. Bermpohl, Z. You, E. H. Lo, H. H. Kim, M. J. Whalen, *J. Cereb. Blood Flow Metabol.* **2007**, *27*, 1806–1818.